Ceramics International 48 (2022) 28181–28190

Contents lists available at ScienceDirect

Ceramics International

journal homepage: www.elsevier.com/locate/ceramint

Fabrication of porous Al_2O_3 ceramics using carbon black as a pore forming agent by spark plasma sintering

Ali Çelik [a,b,*], Gözde Çağlar [a], Yasemin Çelik [b]

[a] Bilecik Seyh Edebali University, Department of Metallurgical and Materials Engineering, 11210, Bilecik, Turkey
[b] Eskişehir Technical University, Department of Materials Science and Engineering, 26555, Eskisehir, Turkey

ARTICLE INFO

Keywords:
Al_2O_3
Porous ceramics
Carbon
Spark plasma sintering (SPS)

ABSTRACT

Fabrication of ceramic materials containing high amount of porosity with controlled size and structure is a critical factor for various applications. In this study, porous alumina ceramics were prepared by addition of 5–30 vol% carbon black (CB) powders with different specific surface area (SSA) into the alumina matrix as a pore forming agent and application of partial sintering via spark plasma sintering (SPS) technique. After removal of CB particles from the ceramic structures, physical, mechanical, and thermal properties of the porous alumina ceramics were investigated. The open porosity level was detected between 38.48 and 59.81% depending on the type and amount of CB removed. The compressive strength of the sintered samples was measured as ~150 MPa, which is ~3 times higher than that of the conventionally sintered samples thanks to the strong neck formation between grains. The large pores formed by removal of CB agglomerates in case of using CB powders with SSA of 107 and 254 m^2/g resulted in a change in thermal conduction mechanism from lattice vibration to thermal convection.

1. Introduction

The porosity is a defect for many structural ceramics since it reduces strength of the materials due to localization of high stresses around pores. On the other hand, porous ceramics are promising for various applications such as filtering of molten metals [1–4], catalyst supports for biomaterials [5–7], thermal insulators [8,9], lightweight parts [10–13], etc., due to their high specific surface area, high permeability, low thermal conductivity, and low density. Depending on the requirements of the corresponding application, it is crucial to fabricate porous ceramics with a controlled pore size and structure. There are different methods reported in the literature for creating porosity in a ceramic body, such as sol-gel synthesis [14–16], direct foaming [17–20], sacrificial pore-forming agents [21–23] and partial sintering [24–26]. Each technique has its own advantages and drawbacks. For instance, the ceramic filters for molten metal filtration were manufactured by the sponge replica technique, which enables one to obtain highly permeable porous ceramics with a total open porosity level in the range of 40–95% and the size between 200 μm and 3 mm [27]. However, the formation of microcracks during pyrolysis of polymeric template is a big problem since it degrades the strength of ceramic filters [28].

Alumina is one of the most well-known ceramic materials in the family of oxide ceramics. Intentional pore-forming in alumina ceramics allows to combine the advantages of porous structures and the unique properties of alumina, such as high thermal and chemical durability at both room and elevated temperatures. Even though all the techniques which are available for the manufacturing of porous ceramics can be utilized to produce porous alumina ceramics, partial sintering and utilizing sacrificial pore forming agents are the most preferred methods. During partial sintering, particles in the compact are bonded to each other at their contact points by diffusion of atoms that is activated by temperature. The properties of the starting precursors and green compact, the partial sintering method to be applied and sintering conditions are the key parameters which affect the size, amount, and distribution of pores in the final product [29]. Hardy and Green [26] investigated the mechanical properties of partially sintered alumina compacts containing 20–40% of porosity depending on the sintering temperature applied between 800 and 1600 °C. They showed a considerable improvement on the fracture toughness, Young's modules and strength values with only 10% increase in densification due to efficient neck formation at the interface of the particles at low partial sintering temperatures (800–1200 °C) [26]. Similarly, Nanjangut et al.

* Corresponding author. Eskişehir Technical University, Department of Materials Science and Engineering, 26555, Eskisehir, Turkey.
E-mail address: acelik@eskisehir.edu.tr (A. Çelik).

https://doi.org/10.1016/j.ceramint.2022.06.121
Received 16 April 2022; Received in revised form 10 June 2022; Accepted 11 June 2022
Available online 14 June 2022

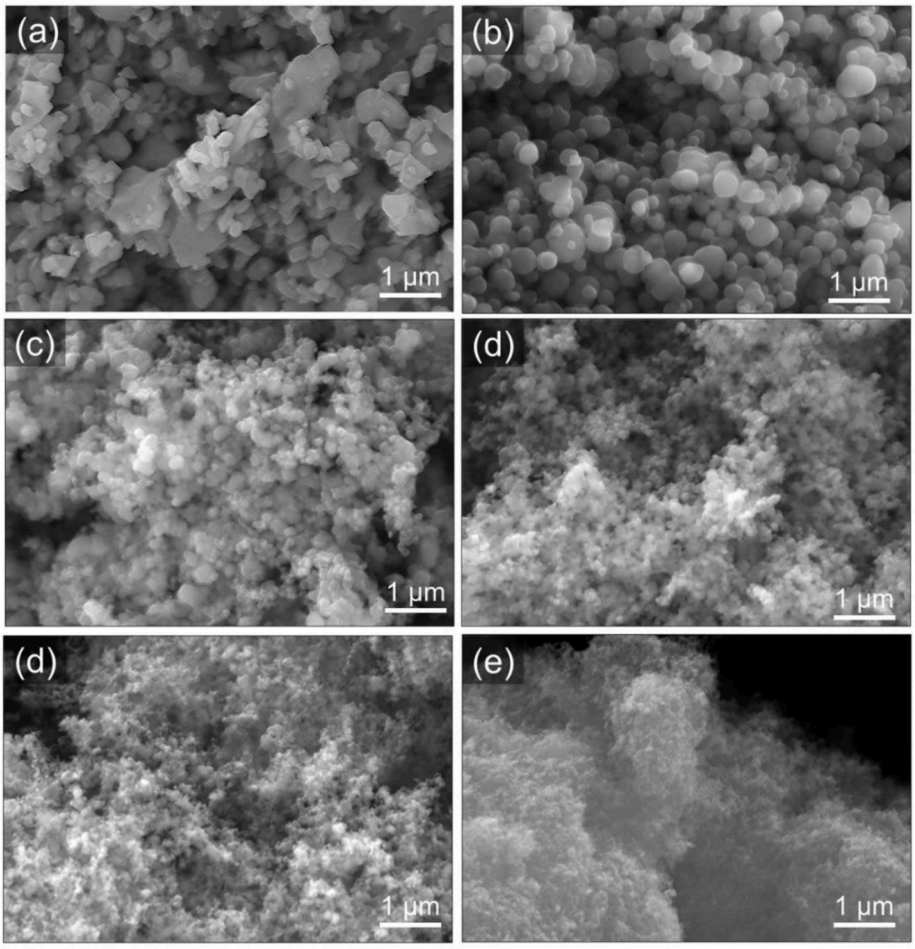

Fig. 1. The micrographs showing the morphology of (a) Al_2O_3, and of CB powders with a SSA of (b) 10 m^2/g, (c) 20 m^2/g, (d) 40 m^2/g, (e) 107 m^2/g and (f) 254 m^2/g.

[30] demonstrated the sharp increase in flexural strength of porous alumina ceramics as a result of neck formation by surface diffusion at relatively low sintering temperatures. The authors reported ~10 times increment in flexural strength for their partially sintered samples while maintaining their %theoretical density (~60%) [30]. Since the way to obtain a high strength porous ceramic by preserving its initial porosity level is to improve the bond strength between particles, Spark Plasma Sintering (SPS) is a promising method for the manufacturing of highly porous structures [31–34]. Jayaseelan et al. [31] fabricated MgO and TiO_2 doped porous alumina ceramics by SPS and reported a relatively high bending strength value (250 MPa) for MgO-doped ceramic with a porosity level of 30% thanks to presence of dopants and efficient bonding between alumina particles during SPS. In another work, Oh et al. [32] manufactured alumina and alumina-SiC composites without using any sintering additives, and compared fracture strength of the ceramics sintered via SPS and hot press (HP). They reported a higher strength for the ceramics sintered by SPS than that of HP, due to the grain refinement and strong neck growth during SPS [32]. In a recent study, Young et al. [34] utilized SPS technique to obtain porous alumina ceramics from alumina granules with an average particle size of 100 μm for filtering applications. After optimizing the neck growth between granules, they tested the filtration capability of the ceramics by filtering graphene solution and burnt soot in wet and dry state, respectively.

The formation of inter-particle necking is critical in the development of porous materials since it determines the strength of the sintered parts as well as functional characteristics such as electrical and thermal conductivity. Therefore, the mechanisms for the formation of inter-particle necks during SPS should be investigated to enable control over the structure and properties of the porous compacts [35]. Langer et al. [36] reported that densification proceeded similarly in sintering of α-Al_2O_3 via SPS and hot pressing (HP) by grain-boundary diffusion mechanism. The advantage of SPS over HP was noted as the formation of higher number of necks during initial stage of SPS due to temperature overshoot. Kun et al. [37] have also shown that SPS enhanced neck growth and accelerated the atom diffusion compared to HP. Recently, Demirskyi et al. [38] have shown that neck growth rate is 100 times faster by SPS than by conventional sintering (CS). Grain-boundary diffusion and power law creep were responsible for neck growth during SPS. Aman et al. [39] made a simple modification of the die and punch assembly to eliminate the effect of mechanical pressure on the neck formation and focused on the characterization of the necking mechanisms at early stages of pressure-less SPS (PL-SPS) in comparison to CS of alumina and copper powdered materials. While no particular necking process (melt or viscous bridge) for alumina powders regardless of the sintering conditions (PL-SPS and CS), even for a very high heating rate 455 °C/min was observed, a non-conventional necking mechanism based on the local mass transfer via surface diffusion or evaporation–condensation in the case of the conductive copper powder was found.

Although partial sintering is a practical method to obtain porous alumina ceramics, the low amounts of porosity and the lack of possibility to control pore shape are the drawbacks of this technique. In order to overcome these limitations, addition of pore-forming agents such as starch [22,40,41], carbon black (CB) [23,42], wheat [43,44], etc. is required. The quasi-spherical CB particles with a wide range of size from

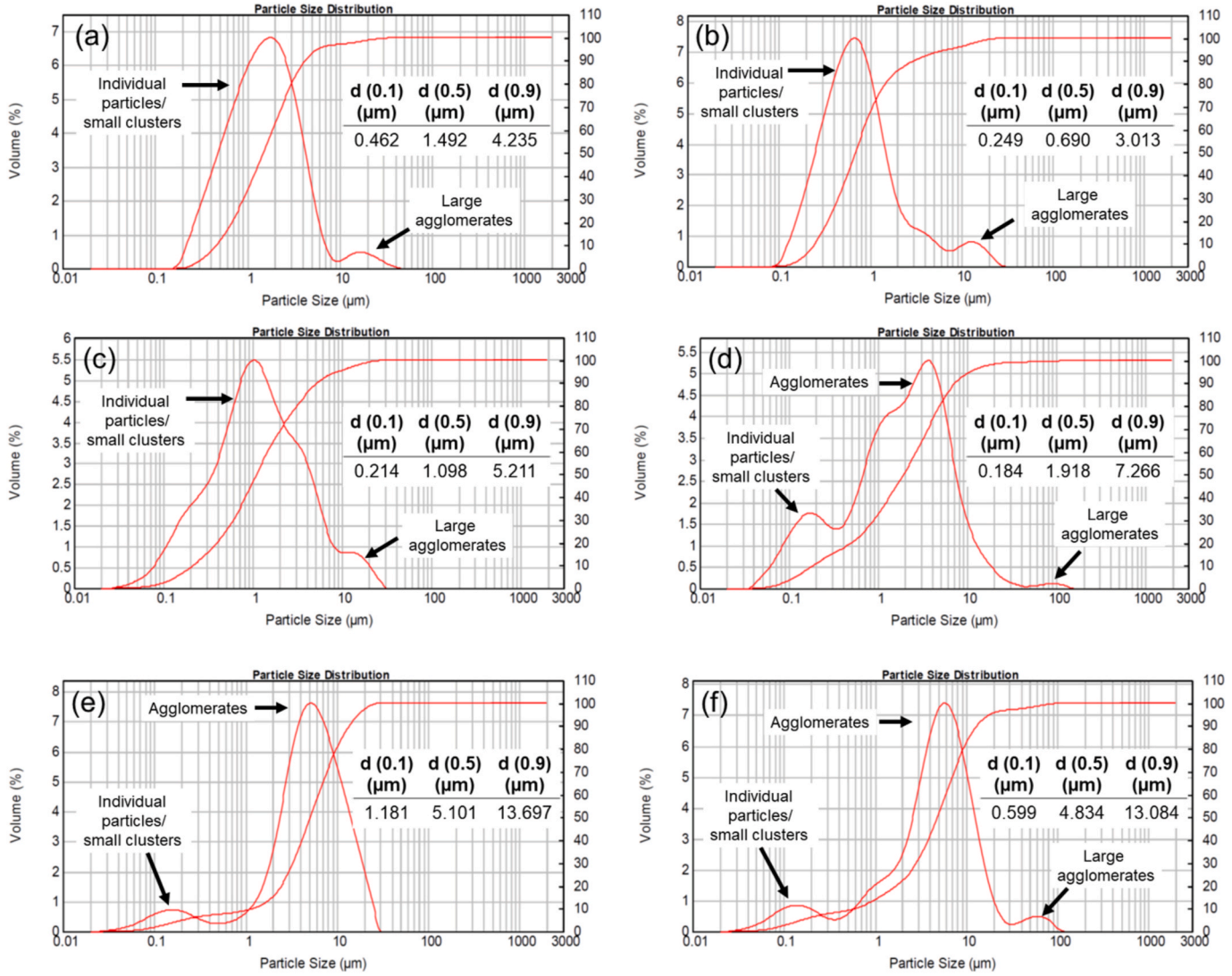

Fig. 2. The average particle size values and the size distribution curves of (a) Al_2O_3 and of CB powders with a SSA of (b) 10 m^2/g, (c) 20 m^2/g, (d) 40 m^2/g, (e) 107 m^2/g and (f) 254 m^2/g.

a few nanometers to hundreds of micrometers are the foremost candidate material as a pore forming agent for alumina ceramics. In addition to their advantageous morphological properties, high purity of CB powders allows to obtain porous ceramics with no residue [42]. Liu et al. [42] examined the thermal and mechanical properties of porous alumina ceramics produced by the addition of N774 grade CB powders in the amounts between 0 and 30 wt%. It was reported that these properties strongly depend on the average pore size distribution, and thermal conductivity and mechanical strength decreased with CB content. The authors suggested to reduce the pore size in order to obtain a thermally insulator and higher strength porous ceramics [42]. As the extension of this study, Liu et al. [23] impregnated alumina sol to the sintered porous alumina ceramics to alter the pore morphology, and observed more than 50% increase in strength compared to porous alumina ceramic with approximately the same amount of porosity (62 vol%) and without any alumina sol.

Although it is possible to successfully produce porous alumina ceramics by using various manufacturing techniques depending on the requirements of a specific application, there is still a demand to improve their mechanical strength and thermal insulation simultaneously. In this study, porous alumina ceramics were prepared by combining two approaches: the addition of CB powders with different specific surface area (SSA) into the alumina matrix as a pore forming agent and application of partial sintering via SPS technique. It was aimed to combine the advantages of the SPS method on strong neck formation during partial sintering to have high strength ceramics and of CB powders to achieve a uniform shape and size distribution of porosities. Prepared samples were characterized in terms of their morphology, density, compressive strength, and thermal diffusivity. The variation of the corresponding properties depending on the amount and SSA of the CB powders was discussed.

2. Experimental procedure

2.1. Preparation of porous ceramics

α-Al_2O_3 powder (Almatis Co.-CT3000-SG) and CB powders with different SSA values (10 m^2/g (Concarb Co.-Grade N990), 20 m^2/g (Gazprom Co.-N772), 40 m^2/g (Yaroslavskiy Co.-N550), 107 m^2/g (Asbury Co.) and 254 m^2/g (Asbury Co.)) were used in the compositions. The microstructures of these precursor powders are shown in Fig. 1. The average particle size values and the size distribution curves of raw powders indicating agglomeration level in each powder batch are also given in Fig. 2. The required amount of α-Al_2O_3 powder and 5–30 vol% CB powders were charged in a planetary mill jar with proper amount of isopropyl alcohol and Si_3N_4 balls (Ø: 3 mm). After mixing at 300 rpm for

Fig. 3. The representative photographs of the alumina samples before and after removal of CB phase.

1 h, the isopropanol was evaporated from the slurries by a vacuum evaporator. The obtained composite powders were then partially sintered by SPS. For this purpose, the required amount of composite powder was placed inside a graphite die (⌀: 14 mm) which was then transferred between the Cu–Be rams of SPS furnace. Rather than selecting a constant sintering temperature, ~40 °C above the temperature at which the first shrinkage observed was selected for the sintering of each composition in order to keep the total degree of densification constant. The pressure was applied as 35 MPa according to the minimum load required to contact the graphite die setup and the rams. The dwell time and heating/cooling rate were selected as 3 min and 50 °C/min, respectively. The sintered samples were designated as AC10, AC20, AC40, AC107 and AC254 depending on the SSA of the CB black powder used in the corresponding composition. After sintering, the ceramics were finally heat treated under atmospheric conditions at 850 °C for 3 h in order to burn-out CB particles from the samples. A representative picture of the samples before and after burn-out process is given in Fig. 3. Conventional sintering was also applied to the prepared composite powders for comparison with SPS method. In this conventional route, the dried powders were compacted in a cylindrical steel die with a height of 20 mm and a diameter of 13 mm under the same pressure applied during SPS to eliminate the effect of different pressing pressure on densification. After compaction, the conventional sintering was performed at 1300 °C, at which the samples showed similar level of shrinkage with the Spark Plasma Sintered (SPSed) counterparts.

2.2. Characterization of porous ceramics

The apparent density ($\rho_{apparent}$) and percent open porosity (*%OP*) of the samples were determined by Archimede's principle (ASTM C373-14) using Eqs. (1) and (2), respectively:

$$\rho_{apparent} = \frac{W_d}{W_w - W_b} \times \rho_{water} \quad (1)$$

$$\%OP = \frac{W_w - W_d}{W_w - W_b} \times 100 \quad (2)$$

where W_d, W_w and W_b are the dry, wet and buoyant weight of the sample and ρ_{water} is the density of distilled water at 25 °C. The theoretical density (ρ_{TD}) of the CB containing composites was obtained by the application of rule of mixtures for density as given in Eq. (3):

$$\rho_{TD} = \rho_{Al2O3} \times V_{Al2O3} + \rho_C \times V_C \quad (3)$$

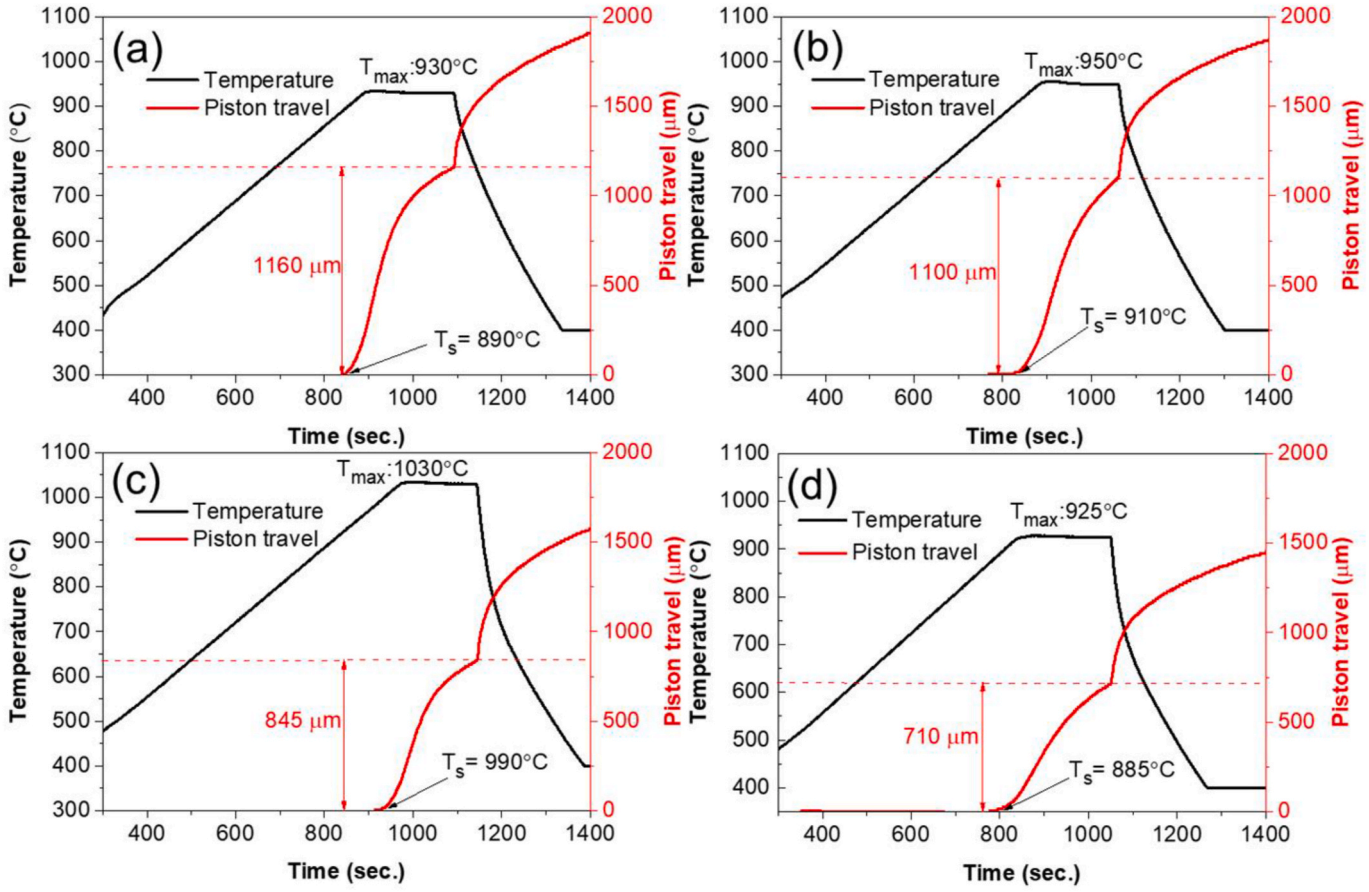

Fig. 4. The shrinkage behavior of AC40 samples containing **(a)** 5%, **(b)** 10%, **(c)** 20% and **(d)** 30% CB powders.

Table 1
The change in theoretical density (TD) and open porosity (OP) before (BCR) and after (ACR) carbon removal for the compositions with different CB content.

	Before carbon removal (BCR)		After carbon removal (ACR)	
	Theoretical density (%ρ_{TD})	Open Porosity (% *OP*)	Theoretical density (%ρ_{TD})	Open Porosity (% *OP*)
Al_2O_3	66.01	33.45	-	-
AC10-5	63.37	35.18	59.93	39.40
AC10-10	64.37	33.44	57.74	41.39
AC10-20	64.46	32.59	51.41	47.34
AC10-30	64.70	31.57	45.23	53.97
AC20-5	60.44	37.99	56.96	42.38
AC20-10	62.81	34.99	56.27	43.03
AC20-20	62.60	34.27	50.15	49.31
AC20-30	61.04	35.14	42.64	56.79
AC40-5	61.27	36.82	58.14	41.40
AC40-10	61.57	36.09	55.38	44.07
AC40-20	59.26	37.42	47.53	51.74
AC40-30	56.13	39.68	39.48	59.81
AC107-5	63.61	34.74	60.11	38.48
AC107-10	64.27	33.15	57.83	39.32
AC107-20	66.71	29.71	50.56	48,48
AC107-30	61.52	34.42	43.10	56,33
AC254-5	64.16	34.06	60.97	38.64
AC254-10	63.79	33.85	59.19	40.61
AC254-20	59.59	37.40	47.72	51.59
AC254-30	54.34	42.67	38.38	58.82

where ρ_{Al2O3} and ρ_C are the theoretical density values of Al_2O_3 (3,96 g/cm^3) and C (2.1 g/cm^3), respectively. The degree of densification (%ρ_{TD}) and percent closed porosity (*%CP*) of the samples were calculated according to Eqs. (4) and (5), respectively:

$$\%\rho_{TD} = \frac{\rho_{apparent}}{\rho_{TD}} \times 100 \quad (4)$$

$$\%CP = (100 - \%TD - \%OP) \quad (5)$$

The microstructures of the samples before and after removal of CB particles (designated by BCR and ACR, respectively) were investigated by the secondary electron detector of a scanning electron microscope (SEM) (Zeiss-Supra 40VP). The compressive strength of the porous samples in parallel to the pressing direction during SPS was determined by a mechanical testing equipment (Instron-5581) under the loading rate of 0.5 mm/min. The thermal diffusivity in both parallel and vertical directions of the samples, with a diameter and height of 14 mm and 2 mm, respectively, was measured via laser flash thermal diffusivity measurement device (Netch- LFA457) between 25 and 350 °C.

3. Results and discussion

3.1. Sintering behavior of porous ceramics

Although SPS is widely used for fabrication of dense structural ceramics, it is also possible to use it for manufacturing of porous ceramics since strong neck formation without losing initial porosity level can be obtained by close monitoring of shrinkage in the compact. In Fig. 4 (a) to (d), piston travel curves depending on shrinkage of AC40 samples containing 5–30% of CB powders during SPS are given representatively. The first movement of the piston was observed at 890 °C (T_s) for AC40-5% sample, and the sintering was carried out at 40 °C above this temperature (T_{max}) (Fig. 4 (a)). While the T_s increased slightly with increasing CB content up to 20%, further addition of carbon black resulted in a considerable reduction on the piston movement temperature (885 °C). This was attributed to the improved electrical conductivity of the samples with higher CB content resulting in a higher electrical current density during sintering [45,46]. Depending on the increase in CB amount, a network of percolating current paths and hot spots were formed within the sample. The temperature of these hot spots can exceed the average temperature of the sample and results in an earlier sliding of particles on each other [46]. The relatively high conductive phase concentration (>20%) required to obtain improved electrical conductivity was assumed to be the result of the slight agglomeration of individual CB particles (Fig. 2 (d)), which increases the percolation threshold level than expected. Moreover, it was observed in the graphs that the total displacement of the piston gradually reduced with an increase in CB content due to restricted densification (shrinkage) of the ceramics by CB particles around alumina grains. The inhibited diffusion in alumina ceramics by carbon-based additives was also reported in Refs. [47,48]. While no direct correlation between the type of CB powder and T_s temperature was detected, the similar trend in shrinkage behavior was also observed for the compositions other than AC40.

Table 1 shows the distribution of %ρ_{TD} and %*OP* of the alumina ceramics before (BCR) and after (ACR) carbon removal stages. It was observed that the average densification of the compositions before carbon removal stage was kept at ~62% with a standard deviation (std. dev.) of ±2.9% for all compositions. This was achieved by applying a specific T_{max} determined for each composition by taking into account the shrinkage onset temperatures (T_s in Fig. 4). It was also observed that %ρ_{TD} tended to decrease with increasing CB amount for the samples with higher SSA CB powders (AC40, AC107, AC254), especially at high CB amounts (30%). While most of the porosities were connected to each other and to the surface (open porosities), the close porosity amount was found as 2.8% in average for the as-sintered samples. After the samples were subjected to heat in air at 850 °C, the CB particles distributed throughout the alumina matrix were removed from the structure as a result of an oxidation reaction; therefore, left additional open porosities behind, which resulted in an increase in total %*OP* with varying amounts (38.48–59.81%) depending on the type and the amount of CB removed (Table 1). These open porosity levels are slightly higher than that of a similar alumina-CB system produced by Lui et al. by conventional sintering [42].

3.2. Microstructural properties of porous ceramics

Fracture surface SEM micrographs of the AC10, AC20, AC40, AC107 and AC254 samples containing 30% CB powder before and after carbon removal stage are given in Figs. 5 and 6, respectively. The spherical CB particles can easily be distinguished from the irregularly shaped much larger alumina grains in the micrographs. While the distribution of CB powders was relatively more homogeneous for the AC10, AC20 and AC40 samples (Fig. 5 (a)–(c)), the CB particles with finer size formed of small agglomerates or large clusters throughout the matrix (Fig. 5 (d) and (e)) due to the inverse relationship between cohesive forces and particle size [49,50]. Accordingly, it was confirmed that the reduction in total shrinkage (shown in Fig. 3) is a result of hindered diffusion by the presence of CB particles in the form of either large clusters or small agglomerates. After post-heat treatment at 850 °C in atmospheric conditions, these CB agglomerates and clusters were removed, creating pores in the structure (Fig. 6). While uniformly distributed pores with gradually decreasing size from AC10 to AC40 samples were observed,

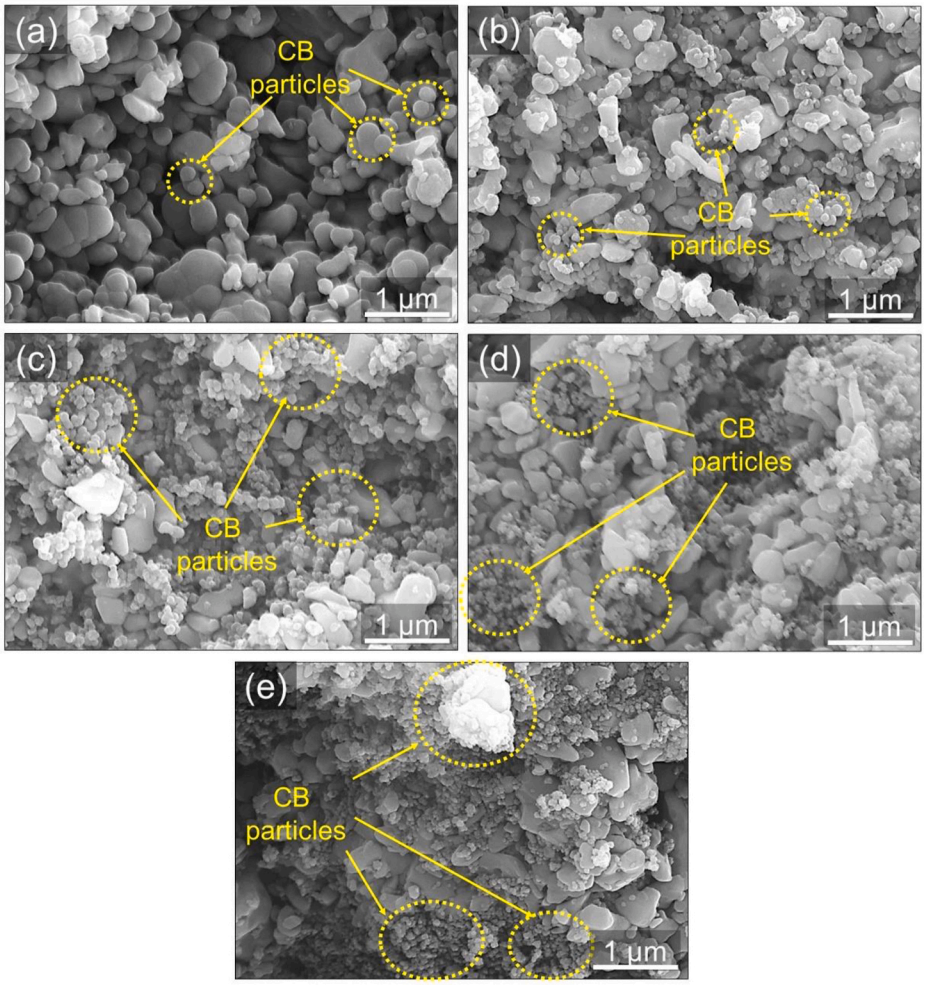

Fig. 5. Fracture surface SEM micrographs of (a) AC10, (b) AC20, (c) AC40, (d) AC107 and (e) AC254 samples containing 30% of CB powder before carbon removal (BCR) stage.

much larger elliptical pores formed in the microstructures of AC107 and AC254 samples due to removal of large clusters that arised from the agglomeration of CB nanoparticles. The ellipticity of these large pores is a result of uniaxial pressing of compacts by the Cu–Be rams during SPS. Consequently, it was proposed that in order for CB powders to be homogeneously dispersed in isopropyl alcohol only by mechanical mixing, without using any surfactants, their surface area should be below 100 m^2/g.

3.3. Mechanical properties of porous ceramics

The representative compressive load-displacement graphs of SPSed AC40 samples with different CB contents and the compressive strength values of the same composition (AC40) sintered by conventional sintering and SPS are presented comparatively in Fig. 7 (a) and (b), respectively. The porous samples containing 5 and 10% of CB exhibited a typically large deformation with increasing load till the occurrence of catastrophic fracture (Fig. 7 (a)). Since these compositions had a relatively lower amount of porosity, their pore wall had a similar structure to a typical dense ceramic and the load-displacement curve showed linearity and a subsequent sudden fracture. On the other hand, the linear behavior of the curves turned to gradual for the samples which contain higher amount of porosity (AC40-20 and AC40-30). This type of behavior is observed highly porous ceramics due to the stepwise collapse of weaker part of each pore wall during loading, as proposed by Pelleg [51]. The compressive strength values of the SPSed samples containing 5 and 10% of CB were measured as ~150 MPa, which is quite similar to the value reported by Jayaseelan et al. [31] for the porous ceramics containing lower amount of porosity (35–38%) sintered by SPS (Fig. 7 (b)). Moreover, these values were found to be ~3 times higher than that of the compressive strength values of the conventionally sintered samples (at 1300 °C for 30 min) with a very close TD%, thanks to the strong neck formation between grains during SPS. When the amount of porosity increased by the addition of higher amount of CB powders (i.e., 20 and 30%), the strength of the SPSed ceramics dropped sharply and became approximately equal to the strength of the conventionally sintered samples. This was attributed to the reduction of pore wall thickness which became effective on the overall compressive strength value of the ceramics.

The compressive strength and theoretical density values of the SPSed porous ceramics depending on CB content are given comparatively in Fig. 8. The strength and %TD of the pure alumina sintered at 950 °C were measured as 285 MPa and 66%, respectively (indicated with an arrow on the graph in Fig. 8). This value is higher than ~93 MPa, which was reported by Liu et al. [42] for their conventionally sintered alumina with a similar porosity level (33%). This indicates how effective the SPS method is in the production of high strength porous alumina ceramics. After introduction of the CB powders into alumina matrix, a remarkable decrease in the strength of the porous ceramics was observed for all the compositions since the amount of porosity increased (Fig. 8). The decrease in strength with increasing porosity amount is consistent with the %TD of the samples (Fig. 8). AC10 compositions with different CB

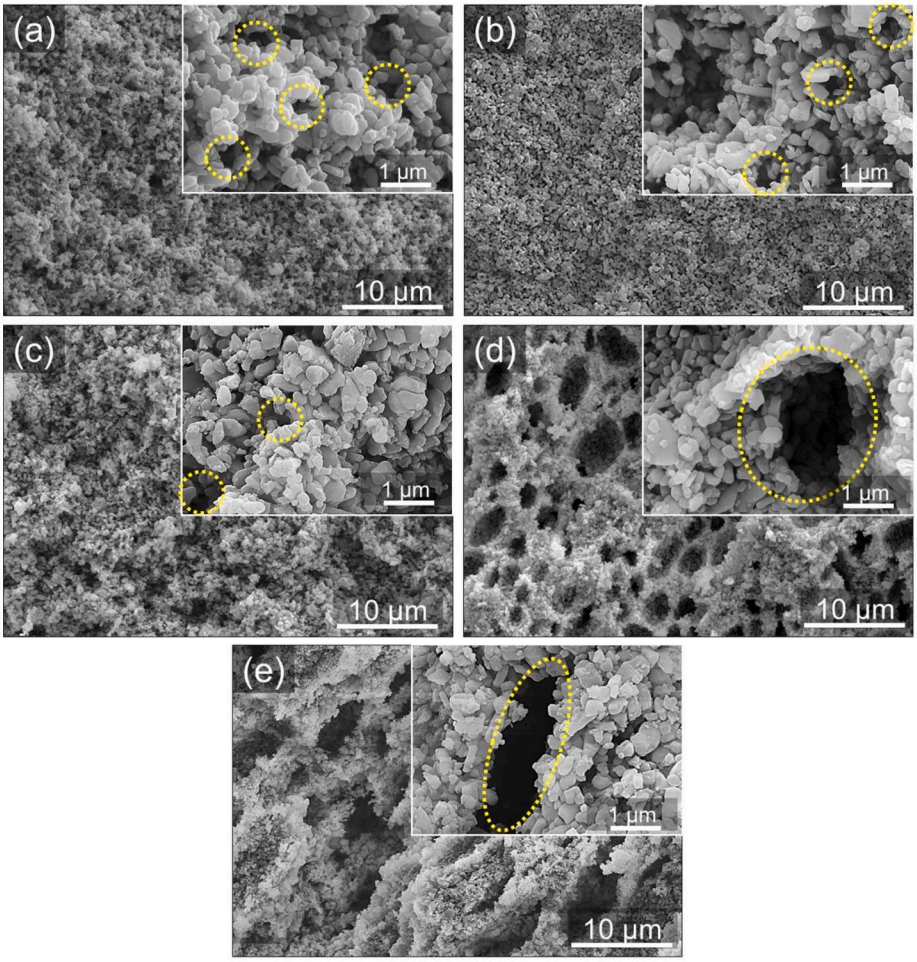

Fig. 6. Fracture surface SEM micrographs of (a) AC10, (b) AC20, (c) AC40, (d) AC107 and (e) AC254 samples containing 30% of CB powder after carbon removal (ACR) stage.

amounts had the highest compressive strength among the others thanks to their relatively larger pores due to larger CB particle size, as well as slightly higher densities. With the reduction of the size of the pores by utilizing low SSA CB powders, the number of pores in a unit volume increased and; therefore, the neck formation between alumina grains was disrupted. On the other hand, the same tendency to decline in strength was not occurred for further increase in specific surface area of CB particles due to considerable agglomeration in the microstructures (Fig. 5). Therefore, the strength of the compositions was remarkably dependent on the amount and the size of the pores, which is the function of the size of either individual CB particles or agglomerates. The compressive strength and porosity of the porous ceramics prepared in this study were compared to those reported in the literature, as shown in Table 2.

3.4. Thermal properties of porous ceramics

Fig. 9(a) shows the change in thermal diffusivity of the SPSed and conventionally sintered AC40 samples with different amounts of CB powders. For the SPSed AC40 samples with different CB content at which the heat is mainly transported by lattice vibrations, called phonons, thermal diffusivity values decreased with increasing temperature in accordance with Eucken law, which expresses the dependence of thermal conductivity on temperature for the ceramics and refractory materials [54]. This was attributed to an increase in phonon scattering with increasing temperature [55,56]. It was also observed for these samples that thermal diffusivity values at a specific temperature decreased with increasing CB amount (Fig. 9(a). This is due to an increase in the porosity amount with increasing CB amount which results in a phonon scattering. For the conventionally sintered samples, remarkably low diffusivity values (<0.2 mm^2/s), which contrarily showed a slight increase with further increase in temperature, were observed (Fig. 9(a)). This was the result of significant phonon scattering in these samples due to presence of large, interconnected pores which formed as a result of a relatively weak binding between alumina grains compared to SPSed counterparts. Such a low conductivity of the weakly sintered materials at relatively moderate temperatures (<800 °C) was attributed to the large heat barrier resistances between particles that constitute the ceramic materials [57]. Therefore, heat conduction occurs by collision of molecules in air inside the pores rather than by lattice vibrations in these conventionally sintered samples. The heat conduction by air molecules in the pores was also dominant when the pore size was relatively higher as in the case of AC10 due to the presence of large CB particles, and of AC107 and AC254 due to presence of large agglomerates and clusters that are formed by small CB particles (Fig. 9 (b)). Since the pores in AC20 and AC40 samples were relatively small in comparison to the others, there was still a solid network to conduct the heat with the same mechanism of dense ceramics. On the other hand, the pores formed by the removal of either large individual CB particles (AC10) or clusters (AC107 and AC254), diffusivity of these compositions decreased due to change in heat conduction mechanism from lattice vibration to thermal convection [56]. Since the measurement temperature range was relatively low (25–350 °C), the thermal radiation, which controls the heat conduction at high temperatures (>1500 K) [57], was

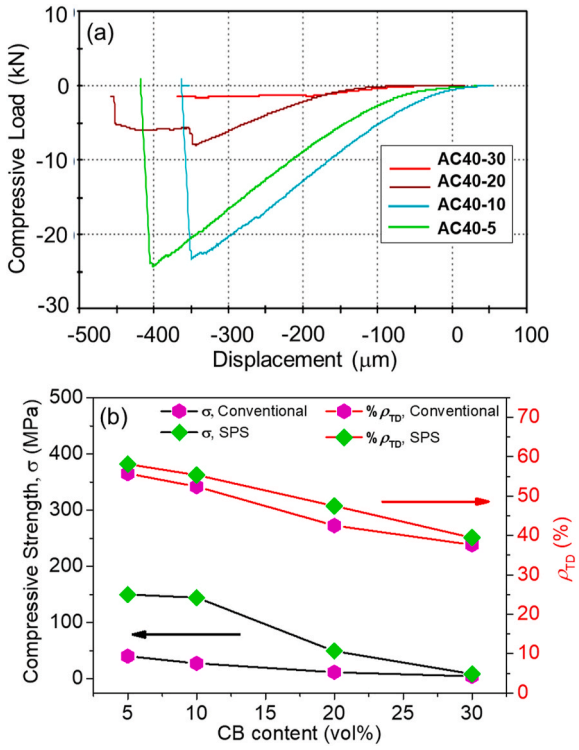

Fig. 7. (a) The load-displacement curves of SPSed AC40 samples and **(b)** the compressive strength of AC40 samples with different CB contents sintered by conventional method and SPS.

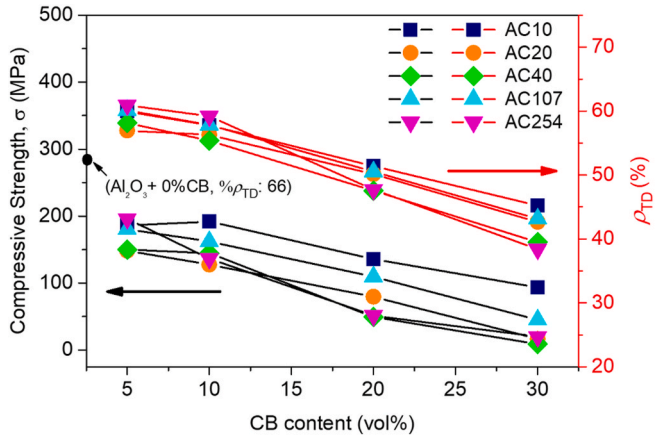

Fig. 8. The comparative compressive strength and relative densification values of the porous alumina ceramics.

not expected to be observed. The pore shape also a parameter which controls the thermal properties of a porous ceramic utilized in applications where thermal insulation is required. Since a uniaxial pressing under a 35 MPa pressure was applied during SPS process in the present study, the pores in the samples were squeezed into an elliptic shape as shown in Fig. 6. This change in the pore shape was expected to alter the thermal behaviors of the samples in the directions vertical and parallel to the pressing axis. Fig. 9 (c) shows the comparative parallel and vertical thermal diffusivity of the AC40 samples with different CB contents. Similar to the conventionally sintered samples, the heat conduction by the gas phase was the dominant mechanism in vertical axis since the necking between the particles in the corresponding direction was so weak to activate the lattice vibration. It is noteworthy to express that the vertical conduction was slightly higher than the conduction in parallel direction for AC40-30 sample.

Fig. 10 gives a summary of the effect of SSA of the CB powders on microstructural, thermal, and mechanical properties of the porous ceramics.

Table 2
Comparison of the strength and porosity level of the porous alumina ceramics with other reports.

Method	Porosity (%)	Compressive Strength (MPa)	Flexural Strength (MPa)
Partial sintering of Al_2O_3 by SPS + pore forming agent as CB (Present work)	38-60	9-196	—
Pore forming agent as carbonized rise husk [21]	25-85	30-125	—
Partial sintering of Al_2O_3 by conventional methods [30]	7-42	–	1-380
Partial sintering of MgO/TiO_2 doped Al_2O_3/3 vol%ZrO_2 by SPS [31]	30-49	—	100-250
Gel casting + pore forming agent as starch [40]	68-81	12-25	—
Partial sintering of Al_2O_3 by conventional method + pore forming agent as CB [42]	33-69	10-93	—
Partial sintering of Al_2O_3 by conventional method [52]	40	170	—
Partial sintering of nano $Al(OH)_3$ by SPS [53]	20-65	up to 400	—

4. Conclusions

In this study, 5–30 vol% CB powders with different SSA were added into the alumina matrix as a pore forming agent. Subsequently, SPS was carried out to fabricate high strength partially sintered porous ceramics. After removal of CB particles from the ceramic structures, physical, mechanical, and thermal properties of the porous ceramics were investigated. Accordingly, the following conclusions were drawn:

- The sintering temperature of the compositions was determined based on the displacement of the Cu–Be piston of the SPS furnace. While an increase in CB content up to 20 vol% retarded the sintering temperature, further increment in CB content caused a reduction in sintering temperature thanks to improved electrical conductivity, which resulted in formation of hot spots locally in the samples.
- 62% in average theoretical density was calculated for the partially SPSed ceramics before removal of CB particles and most of the porosities (~35%) were detected as in open state. After removal of CB, the open porosity level was measured between 38.48 and 59.81% depending on the type and the amount of the CB removed.
- While the distribution of CB powders was relatively homogeneous for the AC10, AC20 and AC40 samples, further reduction in the size of the CB particles caused the formation of agglomerates throughout the structure. Therefore, the specific surface area of CB particles dispersible in isopropanol by only mechanical stirring without using any additional surface-active agents was detected as $<100\ m^2/g$.
- The compressive strength values of the AC40 samples containing 5 and 10% of CB were measured as ~150 MPa, which is ~3 times higher than that of the conventionally sintered samples thanks to the efficient neck formation between alumina grains. When the amount of CB powder further increased, the strength of the SPSed ceramics dropped sharply and became approximately equal to the strength of the conventionally sintered samples. This was attributed to the reduction of pore wall thickness of the ceramics.
- The pores in AC20 and AC40 samples were relatively small and homogeneously distributed compared to the other samples; thus, there was still a solid network to conduct heat by phonons. However, since

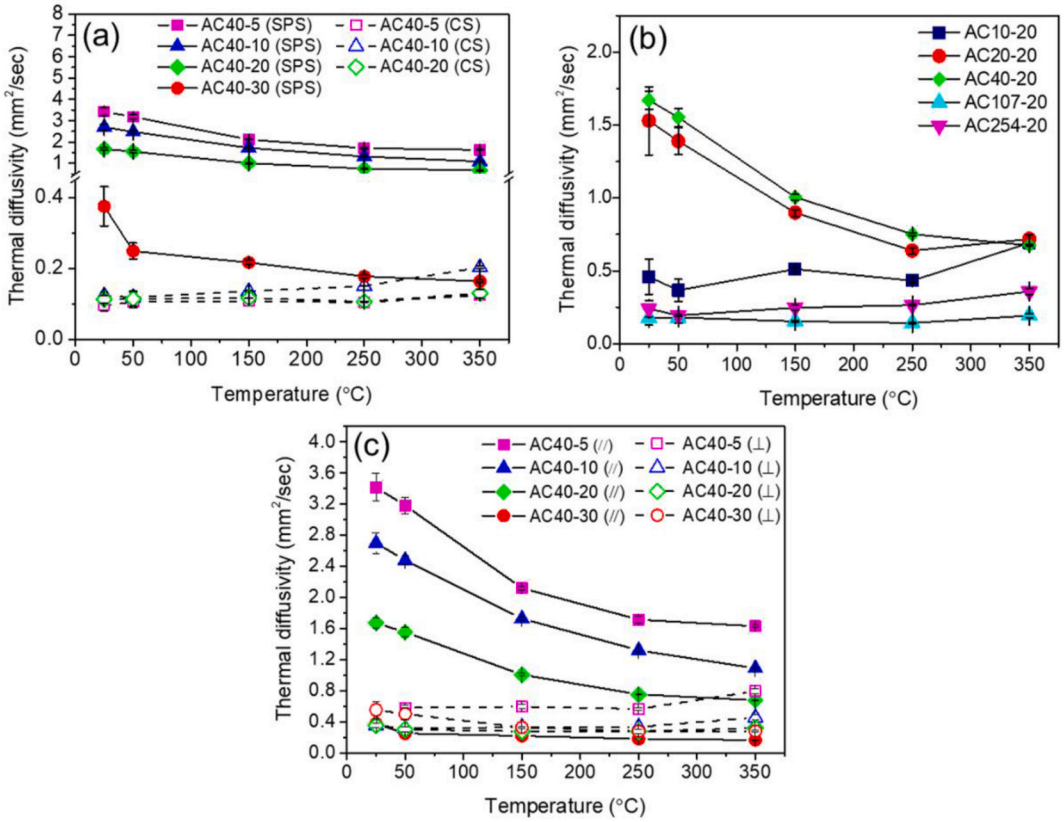

Fig. 9. The thermal diffusivity of the (a) AC40 compositions sintered by conventional and SPS methods, (b) SPSed samples which contain 20% of CB powders with different SSA (c) AC40 compositions in parallel (//) and vertical (⊥) to the pressing direction.

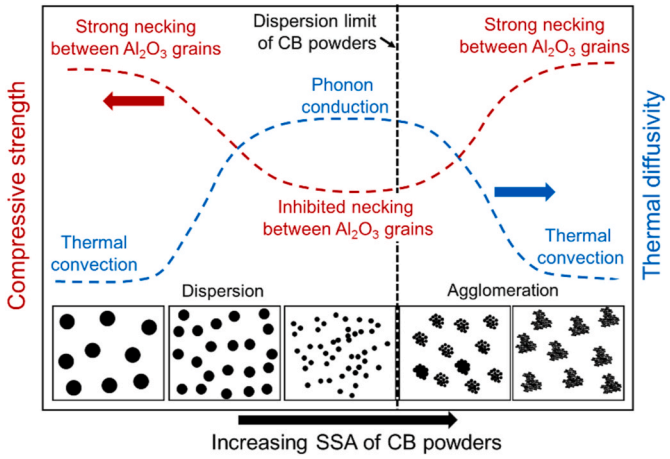

Fig. 10. Summary of the relationship between SSA of CB powders and thermal/mechanical properties of porous ceramics (A color version of this figure can be viewed online). (For interpretation of the references to color in this figure legend, the reader is referred to the Web version of this article.)

the connection between alumina grains was relatively weak for the conventionally sintered samples, scattering in phonon movement became severe, resulting in a heat conduction by collision of air molecules inside the pores in the presence of the large, interconnected porosities. The same mechanism was also observed for SPSed AC10, AC107 and AC254 samples depending on the presence of the larger pores.

Declaration of competing interest

The authors declare that they have no known competing financial interests or personal relationships that could have appeared to influence the work reported in this paper.

Acknowledgement

The financial support for this study by Bilecik Seyh Edebali University Scientific Research Projects Commission (under the project numbers of 2018-02. BŞEÜ.03-05) is gratefully acknowledged.

References

[1] V.N. Antsiferov, Foam ceramic filters for molten metals: reality and prospects, Powder Metall. and Met. Ceram. 42 (9) (2003) 474–476.
[2] L.J. Gauckler, M.M. Waeber, C. Conti, M. Jacob-Duliere, Ceramic foam for molten metal filtration, JMET (J. Med. Eng. Technol.) 37 (9) (1985) 47–50.
[3] A.N. Leonov, M.M. Dechko, Theory of design of foam ceramic filters for cleaning molten metals, Refract. Ind. Ceram. 40 (11) (1999) 537–542.
[4] Z. Taslicukur, C. Balaban, N. Kuskonmaz, Production of ceramic foam filters for molten metal filtration using expanded polystyrene, J. Eur. Ceram. Soc. 27 (2–3) (2007) 637–640.
[5] J.T. Richardson, Y. Peng, D. Remue, Properties of ceramic foam catalyst supports: pressure drop, Appl. Catal. Gen. 204 (1) (2000) 19–32.
[6] U.F. Vogt, L. Györfy, A. Herzog, T. Graule, G. Plesch, Macroporous silicon carbide foams for porous burner applications and catalyst supports, J. Phys. Chem. Solid. 68 (5–6) (2007) 1234–1238.
[7] J.T. Richardson, D. Remue, J.K. Hung, Properties of ceramic foam catalyst supports: mass and heat transfer, Appl. Catal. Gen. 250 (2) (2003) 319–329.
[8] M. Fukushima, Y.I. Yoshizawa, Fabrication of highly porous silica thermal insulators prepared by gelation–freezing route, J. Am. Ceram. Soc. 97 (3) (2014) 713–717.
[9] Y. Zhang, Y. Wu, X. Yang, D. Li, X. Zhang, X. Dong, X. Yao, J. Liu, A. Guo, High-strength thermal insulating mullite nanofibrous porous ceramics, J. Eur. Ceram. Soc. 40 (5) (2020) 2090–2096.
[10] M. Li, A.N. Chen, X. Lin, J.M. Wu, S. Chen, L.J. Cheng, Y. Chen, S.F. Wen, C.H. Li, Y.S. Shi, Lightweight mullite ceramics with controlled porosity and enhanced

properties prepared by SLS using mechanical mixed FAHSs/polyamide 12 composites, Ceram. Int. 45 (16) (2019) 20803–20809.
[11] R. Chen, Y. Huang, C.A. Wang, J. Qi, Ceramics with ultra-low density fabricated by gelcasting: an unconventional view, J. Am. Ceram. Soc. 90 (11) (2007) 3424–3429.
[12] K. Wei, R. He, X. Cheng, R. Zhang, Y. Pei, D. Fang, Fabrication and mechanical properties of lightweight ZrO_2 ceramic corrugated core sandwich panels, Mater. Des. 64 (2014) 91–95.
[13] M. Orlovská, Z. Chlup, Ľ. Bača, M. Janek, M. Kitzmantel, Fracture and mechanical properties of lightweight alumina ceramics prepared by fused filament fabrication, J. Eur. Ceram. Soc. 40 (14) (2020) 4837–4843.
[14] F. Li, X. Huang, J.X. Liu, G.J. Zhang, Sol-gel derived porous ultra-high temperature ceramics, J. Adv. Ceram. 9 (1) (2020) 1–16.
[15] E.P. Simonenko, N.P. Simonenko, E.K. Papynov, O.O. Shichalin, A.V. Golub, V. Y. Mayorov, N.T. Kuznetsov, Preparation of porous SiC-ceramics by sol–gel and spark plasma sintering, J. Sol. Gel Sci. Technol. 82 (3) (2017) 748–759.
[16] K. Tabit, M. Waqif, L. Saàdi, Crystallization behavior and properties of cordierite synthesized by sol-gel technique and hydrothermal treatment, J. Australas. Ceram. Soc. 55 (2) (2019) 469–477.
[17] Z. Du, D. Yao, Y. Xia, K. Zuo, J. Yin, H. Liang, Y.P. Zeng, Highly porous silica foams prepared via direct foaming with mixed surfactants and their sound absorption characteristics, Ceram. Int. 46 (9) (2020) 12942–12947.
[18] Z. Du, D. Yao, Y. Xia, K. Zuo, J. Yin, H. Liang, Y.P. Zeng, Tailoring the microstructure of high porosity Si_3N_4 foams by direct foaming with mixed surfactants, J. Am. Ceram. Soc. 102 (11) (2019) 6827–6836.
[19] H. Khallok, S. Ojala, M. Ezzahmouly, A. Elouahli, M. Jamil, Z. Hatim, Porous foams based hydroxyapatite prepared by direct foaming method using egg white as a pore promoter, J. Australas. Ceram. Soc. 55 (2) (2019) 611–619.
[20] L. Wang, L. An, J. Zhao, S. Shimai, X. Mao, J. Zhang, J. Liu, S. Wang, High-strength porous alumina ceramics prepared from stable wet foams, J. Adv. Ceram. 10 (4) (2021) 852–859.
[21] J. Liu, B. Ren, Y. Lu, X. Xi, Y. Li, K. Liu, J. Yang, Y. Huang, Novel design of elongated mullite reinforced highly porous alumina ceramics using carbonized rice husk as pore-forming agent, Ceram. Int. 45 (11) (2019) 13964–13970.
[22] L. Fu, H. Gu, A. Huang, H. Ni, Correlations among processing parameters and porosity of a lightweight alumina, Ceram. Int. 44 (12) (2018) 14076–14081.
[23] J. Liu, B. Ren, T. Zhu, S. Yan, X. Zhang, W. Huo, Y. Chen, J. Yang, Enhanced mechanical properties and decreased thermal conductivity of porous alumina ceramics by optimizing pore structure, Ceram. Int. 44 (11) (2018) 13240–13246.
[24] Y. Hirata, H. Fujita, T. Shimonosono, Compressive mechanical properties of partially sintered porous alumina of bimodal particle size system, Ceram. Int. 43 (2) (2017) 1895–1903.
[25] E. Gregorová, W. Pabst, V. Nečina, T. Uhlířová, P. Diblíková, Young's modulus evolution during heating, re-sintering and cooling of partially sintered alumina ceramics, J. Eur. Ceram. Soc. 39 (5) (2019) 1893–1899.
[26] D. Hardy, D.J. Green, Mechanical properties of a partially sintered alumina, J. Eur. Ceram. Soc. 15 (8) (1995) 769–775.
[27] M.D. Innocentini, P. Sepulveda, V.R. Salvini, V.C. Pandolfelli, J.R. Coury, Permeability and structure of cellular ceramics: a comparison between two preparation techniques, J. Am. Ceram. Soc. 81 (12) (1998) 3349–3352.
[28] P. Sepulveda, Gelcasting foams for porous ceramics, Am. Ceram. Soc. Bull. 76 (10) (1997) 61–65.
[29] T. Ohji, M. Fukushima, Macro-porous ceramics: processing and properties, Int. Mater. Rev. 57 (2) (2012) 115–131.
[30] S.C. Nanjangud, R. Brezny, D.J. Green, Strength and Young's modulus behavior of a partially sintered porous alumina, J. Am. Ceram. Soc. 78 (1) (1995) 266–268.
[31] D.D. Jayaseelan, N. Kondo, M.E. Brito, T. Ohji, High-strength porous alumina ceramics by the pulse electric current sintering technique, J. Am. Ceram. Soc. 85 (1) (2002) 267–269.
[32] S.T. Oh, K.I. Tajima, M. Ando, T. Ohji, Strengthening of porous alumina by pulse electric current sintering and nanocomposite processing, J. Am. Ceram. Soc. 83 (5) (2000) 1314–1316.
[33] Y. Yang, Y. Wang, W. Tian, Z. Wang, C.G. Li, Y. Zhao, H.M. Bian, In situ porous alumina/aluminum titanate ceramic composite prepared by spark plasma sintering from nanostructured powders, Scripta Mater. 60 (7) (2009) 578–581.
[34] C. Young, C. Zhang, A. Nisar, B. Boesl, A. Agarwal, Spark plasma sintered porous aluminum oxide for filtration applications, Ceram. Int. 47 (15) (2021) 21822–21827.
[35] D.V. Dudina, B.B. Bokhonov, E.A. Olevsky, Fabrication of porous materials by spark plasma sintering: a review, Mater 12 (3) (2019) 541.
[36] J. Langer, M.J. Hoffmann, O. Guillon, Direct comparison between hot pressing and electric field-assisted sintering of submicron alümina, Acta Mater. 57 (18) (2009) 5454–5465.
[37] W. Kun, F. Zhengyi, W. Weimin, W. Yucheng, Z. Jinyong, Z. Qingjie, Study on fabrication and mechanism in of porous metals by spark plasma sintering, J. Mater. Sci. 42 (1) (2007) 302–306.
[38] D. Demirskyi, H. Borodianska, D. Agrawal, A. Ragulya, Y. Sakka, O. Vasylkiv, Peculiarities of the neck growth process during initial stage of spark-plasma, microwave and conventional sintering of WC spheres, J. Alloys Compd. 523 (2012) 1–10.
[39] Y. Aman, V. Garnier, E. Djurado, Pressure-less spark plasma sintering effect on non-conventional necking process during the initial stage of sintering of copper and alumina, J. Mater. Sci. 47 (15) (2012) 5766–5773.
[40] S. Li, C.A. Wang, J. Zhou, Effect of starch addition on microstructure and properties of highly porous alumina ceramics, Ceram. Int. 39 (8) (2013) 8833–8839.
[41] O. Lyckfeldt, J.M.F. Ferreira, Processing of porous ceramics by 'starch consolidation, J. Eur. Ceram. Soc. 18 (2) (1998) 131–140.
[42] J. Liu, Y. Li, Y. Li, S. Sang, S. Li, Effects of pore structure on thermal conductivity and strength of alumina porous ceramics using carbon black as pore-forming agent, Ceram. Int. 42 (7) (2016) 8221–8228.
[43] K. Prabhakaran, A. Melkeri, N.M. Gokhale, S.C. Sharma, Preparation of macroporous alumina ceramics using wheat particles as gelling and pore forming agent, Ceram. Int. 33 (1) (2007) 77–81.
[44] E. Gregorová, W. Pabst, Z. Živcová, I. Sedlářová, S. Holíková, Porous alumina ceramics prepared with wheat flour, J. Eur. Ceram. Soc. 30 (14) (2010) 2871–2880.
[45] U. Anselmi-Tamburini, S. Gennari, J.E. Garay, Z.A. Munir, Fundamental investigations on the spark plasma sintering/synthesis process: II. Modeling of current and temperature distributions, Mater. Sci. Eng. A 394 (1–2) (2005) 139–148.
[46] O. Guillon, J. Gonzalez-Julian, B. Dargatz, T. Kessel, G. Schierning, J. Räthel, M. Herrmann, Field-assisted sintering technology/spark plasma sintering: mechanisms, materials, and technology developments, Adv. Eng. Mater. 16 (7) (2014) 830–849.
[47] I. Akin, Investigation of the microstructure, mechanical properties and cell viability of zirconia-toughened alumina composites reinforced with carbon nanotubes, J. Ceram. Soc. Jpn. 123 (1437) (2015) 405–413.
[48] J. Echeberria, N. Rodríguez, J. Vleugels, K. Vanmeensel, A. Reyes-Rojas, A. Garcia-Reyes, C. Dominguez-Rios, A. Aguilar-Elguezabal, M.H. Bocanegra-Bernal, Hard and tough carbon nanotube-reinforced zirconia-toughened alumina composites prepared by spark plasma sintering, Carbon 50 (2) (2012) 706–717.
[49] C. Pomchaitaward, I. Manas-Zloczower, D.L. Feke, Investigation of the dispersion of carbon black agglomerates of various sizes in simple-shear flows, Chem. Eng. Sci. 58 (9) (2003) 1859–1865.
[50] M.E. Spahr, R. Rothon, Carbon black as a polymer filler, in: R. Rothon (Ed.), Fillers for Polymer Applications, Polymers and Polymeric Composites: A Reference Series, Springer, Cham., 2017, pp. 262–290.
[51] J. Pelleg, Mechanical Properties of Ceramics, vol. 213, Springer Science & Business, 2014, pp. 72–76.
[52] Y. Hirata, T. Shimonosono, T. Sameshima, S. Sameshima, Compressive mechanical properties of porous alumina powder compacts, Ceram. Int. 40 (1) (2014) 2315–2322.
[53] D. Chakravarty, H. Ramesh, T.N. Rao, High strength porous alumina by spark plasma sintering, J. Eur. Ceram. Soc. 29 (8) (2009) 1361–1369.
[54] E.Y. Litovsky, M. Shapiro, Gas pressure and temperature dependences of thermal conductivity of porous ceramic materials: Part 1, Refractories and ceramics with porosity below 30, J. Am. Ceram. Soc. 75 (12) (1992) 3425–3439.
[55] D.R. Flynn, Thermal conductivity of ceramics, in: J.B. Wachtman (Ed.), Mechanical and Thermal Properties of Ceramics, vol. 303, NBS Spec. Publ, 1969, pp. 63–123.
[56] L. Hu, C.A. Wang, Z. Hu, S. Lu, C. Sun, Y. Huang, Porous yttria-stabilized zirconia ceramics with ultra-low thermal conductivity, Part II: temperature dependence of thermophysical properties, J. Mater. Sci. 46 (3) (2011) 623–628.
[57] E. Litovsky, M. Shapiro, A. Shavit, Gas pressure and temperature dependences of thermal conductivity of porous ceramic materials: Part 2, Refractories and ceramics with porosity exceeding 30%, J. Am. Ceram. Soc. 79 (5) (1996) 1366–1376.